Journal of Luminescence 277 (2025) 120936

Contents lists available at ScienceDirect

Journal of Luminescence

journal homepage: www.elsevier.com/locate/jlumin

Full Length Article

Unravelling the luminescence spectrum of garnet grossular var. tsavorite: The role of chromium (III), manganese (II) and misattribution of vanadium (II)

A. Idini [a,c,*], R. Argazzi [b], F. Frau [c], M. Fantauzzi [c], C. Angeli [d]

[a] Department of Chemical, Physical, Mathematical and Natural Sciences, University of Sassari, Italy
[b] CNR-ISOF c/o Department of Chemical, Pharmaceutical and Agricultural Sciences, University of Ferrara, Italy
[c] Department of Chemical and Geological Sciences, University of Cagliari, Italy
[d] Department of Chemical, Pharmaceutical and Agricultural Sciences, University of Ferrara, Italy

ARTICLE INFO

Keywords:
Tsavorite fluorescence
UV-SW yellow emission by Mn(II)
UV-LW red emission by Cr(III)
Oxidation state of vanadium
Oxidation state of manganese

ABSTRACT

Gem quality garnet var. tsavorite from Tanzania is investigated by means of SEM-EDS, XPS and fluorescence spectroscopy to decipher its luminescence spectrum. The EDS analysis confirms that the main constituents of the tsavorite samples from Tanzania are those of grossularia (i.e. Ca, Al, Si, O), with V, Mn, Cr, Ti and Mg as minor but characteristic elements (particularly V, Mn and Cr) of the tsavorite variety. The XPS analysis shows that the oxidation state of Mn is +2 and that of V is +3. The luminescence of tsavorite in the yellow region (591 nm) is originated by Mn^{2+} in dodecahedral coordination (D_2 point symmetry) while the luminescence in the red region (690–750 nm) is originated by Cr^{3+} in octahedral coordination (O_h point symmetry) in a strong crystal field. Contrary to what is often reported in the literature, this study demonstrates that V^{2+} (or other 3d transition metal ions as well) is not responsible for the red emissions of tsavorite.

1. Introduction

Tsavorite is a vanadium (V) - manganese (Mn) bearing variety of grossular, with titanium (Ti), magnesium (Mg), and chromium (Cr) as common minor elements ([1], Julien Feneyrol et al., 2014, [2]). Tsavorite, especially coming from Kenya and Tanzania (Bridges, 1974), drew the attention of gemmologists due to the high value of its spectacular green-coloured crystals [3] caused by its vanadium and chromium content [4]. Tsavorite has been investigated by petrologists due to its geological provenance from the Neoproterozoic Mozambique Mobile Belt [5], for its peculiar metamorphic genesis at expense of evaporite protoliths [6], and was used also to date global tectonic events, such as the final amalgamation of Gondwana supercontinent [7]. Tsavorite has an uncommon feature for a natural garnet: a visible yellow and red fluorescence upon excitation with UV wavelength light [2,8]. Tsavorite luminescence spectrum was first studied by Mazurak & Czaja [9], and two different explanations have been proposed with regard to the origin of the emission centres in the red region. The first explanation identifies Cr^{3+} as an emission centre, due to the identical spectrum of Cr^{3+} in grossular [10]. However, Czaja & Mazurak [10] did not present the full chemical analysis of the sample, hence other options than Cr^{3+} were not even discussed. The second explanation claims that V^{2+} is the origin of some emissions in the 680–720 nm region [11], although the oxidation state of V in tsavorite was already determined as +3 [12] through synchrotron light (K-edge X-ray absorption spectra). In order to introduce our study, a detailed reconstruction of the bibliographical support of this hypothesis is mandatory. In Gaft et al. [11], precisely in Fig. 10c and Fig. 12c–d, the similarity between the excitation spectrum of a synthetic garnet (gadolinium gallium garnet GGG: Zr^{4+}; Cr^{3+}) and the absorption spectrum of tsavorite are considered a clue to the presence of V^{2+}, but this similarity is far to be effectively recognized in the above-mentioned figures. Moreover, in the absorption spectrum of tsavorite, Cr^{3+} is not even considered as possible chromophore centre. Another supposed evidence of the role of V^{2+} proposed by Gaft et al. [11] came from Gaft et al. [13]. Here the authors studied the luminescence of natural sillimanite (Al_2SiO_5) containing respectively tens and hundreds mg/kg of V and Cr, and just a few mg/kg of Mn. They analysed the decay time of the emissions and stated that other 3 d^3 ions than Cr^{3+} could be the possible emission origin in the red region, proposing Mn^{4+} and/or V^{2+}. However, the authors themselves showed that in the equivalent synthetic

* Corresponding author. Department of Chemical, Physical, Mathematical and Natural Sciences, University of Sassari, Italy.
E-mail address: aidini@uniss.it (A. Idini).

https://doi.org/10.1016/j.jlumin.2024.120936
Received 7 June 2024; Received in revised form 6 October 2024; Accepted 10 October 2024
Available online 11 October 2024

sillimanite these emissions related to Mn^{4+} and V^{2+} were not observed. Despite the lack of direct experimental observations, the following sentence *"the luminescence spectra of supposedly Mn^{4+} and V^{2+} in sillimanite"* [13] has been considered as a certainty in several papers and for different minerals afterwards.

In an old research paper [14], the V^{2+} emission was supposed based on the absorption spectra of a natural beryl from Minas Gerais, Brazil. However, the full elemental composition of this natural sample was not presented, and only the presence of V was reported. As a consequence, the absorption spectra were interpreted considering V as the unique explanation of luminescence, while the beryl from Minas Gerais also contains Cr^{3+} [15]. Lastly, in the recent work of Zhang et al. [8] electron paramagnetic resonance spectroscopy (EPR) analysis shows that V in tsavorite is V^{3+} and the authors also observe that the luminescence signal is suppressed as the V content increases.

For all the incongruities above mentioned concerning Cr, V and Mn, the aim of this work is to unravel the luminescence spectrum of tsavorite, taking advantage of the results of X-ray energy dispersive spectroscopy (EDS) and X-ray photoelectron spectroscopy (XPS) techniques in order to discuss the origin and nature of the emissions.

2. Experimental

The tsavorite samples (Fig. 1) were purchased directly from D-Block mine, Merelani Hills, Northern Tanzania (https://www.mindat.org/loc-189433.html). The most euhedral and inclusion-free crystals were used for analysis.

Scanning electron microscope (SEM) equipped with an energy-dispersive X-ray spectrometer (EDS) was used for imaging and elemental characterization of the crystals at the University of Sassari (Italy) (Model Zeiss EVO LS 10, SSD detector INCA X-act model SI-ADD0048 Oxford Instruments). The SEM operating conditions are listed in Table 1. The EDS acquisition time for the quantitative analyses was 180 s, and the current probe was in the range 0.582–0.612 nA.

For quantitative and unnormalized elemental chemical data, the EDS spectra were processed with the AZTec® 6.1 HF4 software suite using the Smithsonian Microbeam Standards Datasheets.

X-ray photoelectron spectroscopy (XPS) analyses were performed at the University of Cagliari (Italy), using a Thetaprobe spectrometer

Fig. 1. The tsavorite samples studied in this work. The specimens come from D-Block mine, Merelani Hills, Tanzania.

Table 1
Operating conditions for scanning electron microscopy.

SEM operating conditions	Samples			
	Ts A	Ts B	Ts C	
Acc. Voltage (kV)	20	20	20	20
Magnification	2530x	1865x	4990x	870x
Working distance (mm)	7.8	9.5	8.8	9.3
Pixel size (μm)	0.05451	0.07395	0.02764	0.15853
Dwell time (μs)	5	10	5	10

(Thermo Fisher Scientific, Walman, US) equipped with a monochromatic Al Kα X-ray source ($h\nu = 1486.6$ eV). The tsavorite sample was mounted after wiping with water and isopropanol in order to remove soluble salts and part of the organic contamination layer due to handling. The spectra were acquired in constant analyzer energy mode using a pass energy of 200 eV and 100 eV for survey and high-resolution spectra respectively. The linearity of the binding energy scale of the spectrometer was periodically checked according to ISO 15472:2010. The energy resolution with the 100 eV pass energy was found to be 0.93 ± 0.05 eV, corresponding to the full width at the half maximum height of Ag $3d_{5/2}$ signal acquired during the spectrometer calibration.

To compensate for sample charging, a flood gun was used, and the binding energy values were referenced to the C1s peak of adventitious aliphatic carbon at 285.0 eV.

The spectra were processed with CasaXPS software (version 2.3.25PR1.0) (Fairley et al., 2021).

Tsavorite emission spectra, both at room temperature (296 K) and liquid nitrogen temperature (77 K), were recorded at the University of Ferrara, with an Edinburgh Instruments FS920 steady state spectrofluorometer configured with a 450 W xenon short arc lamp as excitation source, a TMS300-X single excitation monochromator supplied with a 1800 g/mm grating blazed at 250 nm (300 mm focal length, f/4.1 aperture, 1.8 nm/mm linear dispersion), a double emission monochromator consisting of two coupled 300 mm focal length, f/4.1 monochromators supplied with 1200 g/mm gratings blazed at 500 nm (1.35 nm/mm linear dispersion) and a universal sample chamber. A red sensitive photomultiplier (Hamamatsu R928P) in a standard uncooled housing mounted at the exit port of the second stage of the emission monochromator was used as detector in the 200–850 nm wavelength interval. Tsavorite crystals (Ts A, Ts C, Fig. 1) of approximately 5 mm in diameter were placed in a cavity milled in a blackened aluminium block, cut at 30° with respect to the excitation beam, and fitted in the sample holder of an Oxford Instruments cryostat connected to a DTC-2 temperature controller. The fluorometer was PC controlled through a proprietary Edinburgh Instruments F900 software providing emission spectra factory corrected for instrument response by means of a halogen lamp of known irradiance. Typically, a spectral bandwidth of 1 nm was used for each measurement.

3. Chemical features

The backscattered electron (BSE) images of the tsavorite faces show that the regions analysed are homogeneous in all the samples Ts A, Ts B, and Ts C (Fig. 2), hence excluding the presence of other included minerals or elemental zoning.

The EDS spectra show all the grossular elemental constituents (O, Ca, Si, Al) and minor elements typical of tsavorite (V, Mn, Cr, Ti and Mg) (Table 2 and Table S1 in the supplemental material).

The average values of the major elements are close to the stoichiometric values of the grossular (i.e., SiO_2 40.02 wt%; CaO 37.35 wt%; Al_2O_3 22.64 wt%). The minor elements V, Mn, Cr, Mg and Ti are detectable in 43, 43, 41, 39, 36 out of 43 analyses, respectively.

The representative quantitative analysis shows that the compositions are very close to the tsavorite chemistry of the whole crystals [2,16], but with iron that was below the detection limit (Table 3).

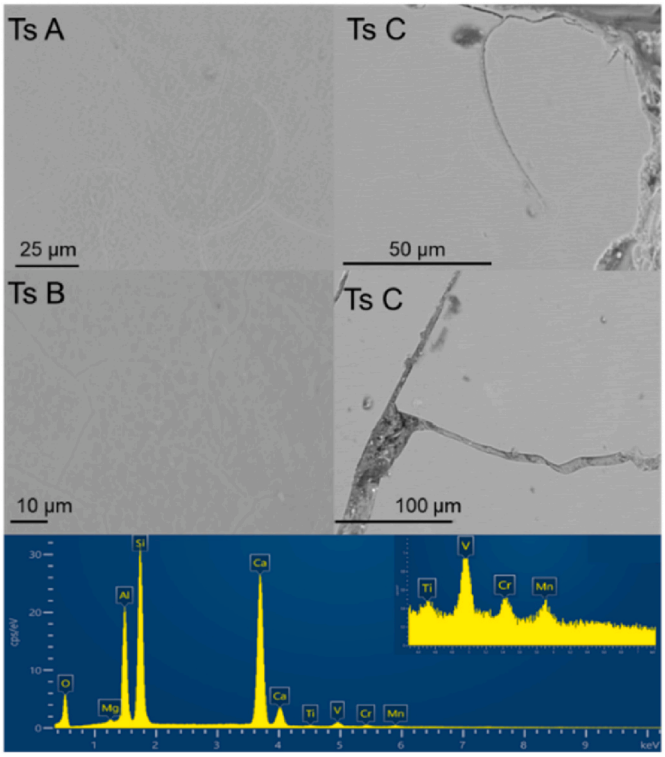

Fig. 2. Backscattered electron images of the tsavorite crystal faces analysed in this work. On the bottom, a representative EDS spectrum and the onset with the detail of the Ti-V-Cr-Mn Kα energies.

The contents of V, Mn and Cr can be used within the classification scheme proposed by Feneyrol et al. [17]: the tsavorite here presented falls into the type 2 (V > Mn > Cr) (Fig. 3) coherently with the data of other studies on Tanzanian tsavorite [17].

The XPS survey spectra of the crystal surface showed the presence of signals from Si, O, Al, Ca and carbon. The presence of carbon is ascribed to the organic hydrocarbon layer that is always present at the surface of samples exposed to the atmosphere. The signals of Mg, Mn and V were also detected (Fig. 4). Unlike the EDS analysis, sodium, zinc and fluorine were observed, while Cr and Ti were likely below the instrumental detection limit. The binding energy values of the most intense peak of the main elements are reported in Table 4.

The high-resolution spectra of the most abundant elements, Si 2p, Al 2p, O 1s and Ca 2p, are shown in the supplementary information file (Fig. S1).

Si 2p is curve fitted with a doublet due to spin-orbit coupling; the energy separation between the Si $2p_{3/2}$ and Si $2p_{1/2}$ components is 0.7 eV and the area ratio is 2:1. The binding energy of the Si $2p_{3/2}$ component is 102.5 (0.1) eV and it is in agreement with the value reported by Poon et al. (2020) for Si $2p_{3/2}$ in the surface region of a polished almandine garnet. Similarly, the binding energy value of Al 2p (75.3 (0.1) eV) is in agreement with the value reported for Al in the same article (Poon et al., 2020). O 1s shows the presence of two components: the one at 530.5 (0.1) eV is ascribed to oxygen in the silicate (Poon et al., 2020); the second and less intense component found at 531.6 (0.2) eV might be due to the presence of -OH groups at the surface of the sample (Fantauzzi et al., 2010) or related to the documented hydrogarnet substitution in tsavorite [17]. Ca 2p is constituted by a doublet due to spin-orbit coupling; the energy separation between the Ca $2p_{3/2}$ and Ca $2p_{1/2}$ components is 3.5 eV and the area ratio is 2:1. The binding energy of Ca $2p_{3/2}$ peak was found to be 346.5 (0.2) eV. Mn $2p_{3/2}$ signal was curve fitted considering the multiplet splitting of Mn^{2+} due to coupling of unpaired 2p-electron after photoemission with unpaired 3d electrons. Following the multiplet splitting approach for the Mn $2p_{3/2}$ peak, five synthetic components with the same full width at half maximum (FWHM) were considered together with a shake-up satellite (Fig. 5a). The area of each component of the multiplet splitting was constrained according to Biesinger et al. (2011), while the binding energy of each component was let free to vary (Table S1). Small differences are found compared to the values reported for MnO by Biesinger et al. (2011), and these differences might be due to a ligand effect that can shift the energy of the final-states (Grosvenor et al., 2016). The presence of the shake-up satellite is also typical for Mn^{2+} (Biesinger et al., 2011; Grosvenor et al., 2016). The binding energy of the multiplet splitting peaks and of the shake-up satellite and the curve fitting parameters are reported in the supplementary material file (Table S2). The curve fitting of Fe 2p signal was not attempted due to the poor signal to noise ratio (Figure S2).

Regarding vanadium, the binding energy of the V $2p_{3/2}$ signal was found to be 515.4 (0.2) eV (Fig. 5b). This binding energy value is in good agreement with the value reported by Silversmit et al. (2004) for V^{3+}. The presence of V as V^{3+} observed with XPS is in full agreement with EPR [8] and XAS analysis on tsavorite samples [12].

Considering the elemental composition from EDS analysis and the oxidation state of Mn and V (+2 and + 3 respectively) from XPS analysis, the recast of garnet end-member [18] can be calculated following the method developed by Locock [19] (Table 5; Table 6)

Besides grossular, which accounts for 84.46–86.91 mol %, the highest values are for goldmanite (4.86–7.25 mol %) due to the V^{3+} occupancy of the octahedral site, followed by uvarovite (0.95–1.55 mol %) and spessartine (1.12–1.50 mol %) due to the Mn^{2+} occupancy of the dodecahedral site (Table 6).

Table 3
Elemental composition by EDS of the tsavorite here studied compared with the bulk composition from Ref. [2][a]. bdl = below detection limit.

oxide wt %	Tsavo M[a]	Tsavo T[a]	Ts A1	Ts B1	Ts C6	Ts C1	Ts C2
	bulk	bulk	point	area	point	point	point
SiO_2	38.7	38.9	38.39	38.59	38.91	38.79	39
TiO_2	0.33	0.3	0.29	0.3	0.22	0.26	0.32
Al_2O_3	20.98	21.15	20.11	20.52	20.27	20.66	20.69
Cr_2O_3	0.02	0.02	0.39	0.34	0.32	0.46	0.42
V_2O_3	1.32	1.24	2.35	1.96	1.95	1.62	1.83
FeO	0.39	0.12	bdl	bdl	bdl	bdl	bdl
MnO	0.33	0.34	0.68	0.52	0.58	0.59	0.53
MgO	0.56	0.35	0.34	0.3	0.31	0.29	0.31
CaO	35.1	35.7	34.82	36.56	36.73	36.86	36.71
Total	97.73	98.12	97.37	99.09	99.29	99.53	99.81

Table 2
Statistic of the elemental composition in wt% of tsavorite studied in this work. Full data are reported in table S1 of the supplemental material.

Statistic	SiO_2	CaO	Al_2O_3	MnO	V_2O_3	TiO_2	MgO	Cr_2O_3
43 analyses				43 of 43	43 of 43	36 of 43	39 of 43	41 of 43
Max	40.12	43.65	21.22	0.81	2.86	0.42	0.46	0.6
Min	34.03	34.82	17.6	0.52	1.62	0.22	0.17	0.31
Average	37.93	38.5	19.89	0.65	2.07	0.31	0.32	0.41
Std. Dev	1.82	2.26	1.06	0.1	0.3	0.11	0.1	0.12

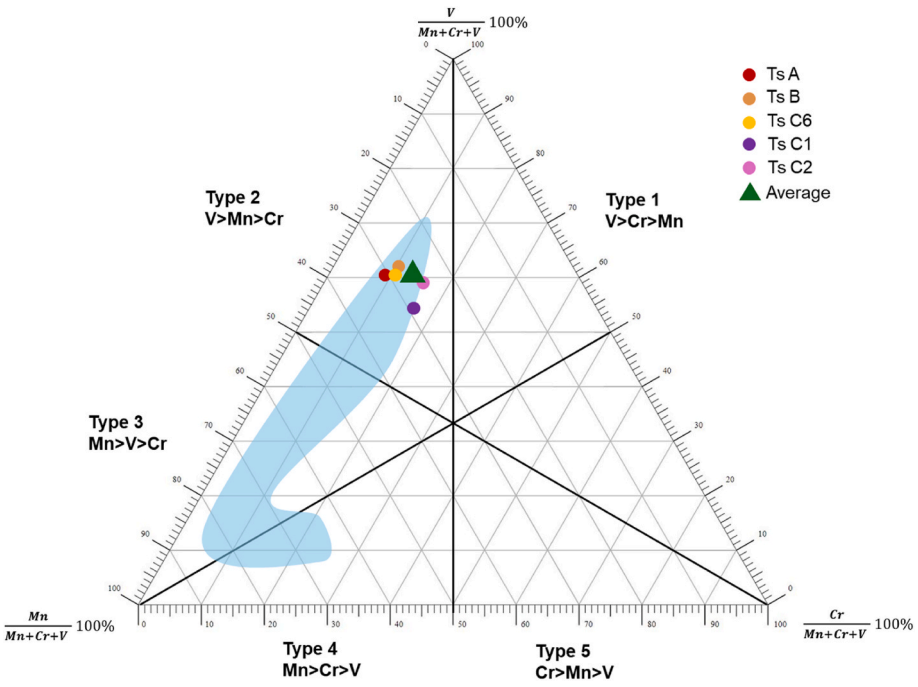

Fig. 3. Classification ternary diagram of tsavorite based on the relative contents of vanadium, manganese, and chromium. Pale-blue area represents the data from literature of Tanzanian tsavorite [17].

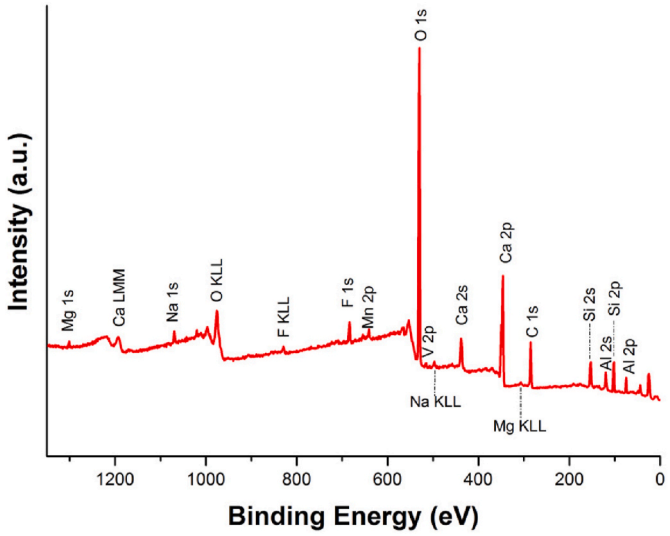

Fig. 4. XPS survey spectra of the tsavorite sample. X-ray source: Al Kα.

Table 4
Binding Energy values (eV) of the main photoelectron peaks for the elements detected at the surface of the tsavorite sample. Mean values over three measurements on three different areas of the sample (P1-3), and standard deviation (s.d.) are also reported.

Signal	Binding Energy (eV)
Al 2p	75.3 (0.1)
O 1s $_{silicate}$	530.5 (0.1)
O 1s $_{hydroxide}$	531.6 (0.2)
Si $2p_{3/2}$	102.5 (0.1)
Ca $2p_{3/2}$	346.5 (0.2)
Na 1s	1070 (0.2)
F 1s	684.6 (0.1)
Mn $2p_{3/2}$	640.2 (0.1)
V $2p_{3/2}$	515.4 (0.2)

4. Luminescence features

The tsavorite luminescence emission spectra at 77 K and 296 K acquired under excitation light at 408 nm are shown in Fig. 6. The crystal has two distinct emission centres [2] which lead to two structures in the emission spectrum: (i) one broad band peaking at 591 nm, thus in the yellow-orange region and (ii) a complex set of convoluted bands in the far-red region (695–755 nm)

4.1. Yellow-orange region

The broad emission centered at 591 nm does not change as temperature decreases. Its emission centre could be confidently attributed to Mn^{2+} due to the well-known fluorescence caused by the $Mn^{2+} \leftrightarrow Ca^{2+}$ substitution in various minerals (Gorobets & Rogojine, 2001) and in synthetic garnets [20]. It is noteworthy to point out that the Mn^{2+} occupancy of the X site of garnets has been known for years in the mineralogical literature [18], recently confirmed by the work of Taran et al. [21] where an extensive discussion is dedicated to the crystallographic role of Mn in garnet and to the analysis of its spin-forbidden emissions: Mn^{2+} ions occupy a distorted dodecahedral site (point symmetry D2) [22]. Only recently the same topic has been described in the inorganic chemistry and material science literature of synthetic garnets [23]. In the excitation spectrum of the emission at 591 nm (Fig. 7) five bands are recognized at 296 K, three narrow bands peaking at 408, 419 and 429 nm and two broad bands at 451 and 474 nm.

The three photoluminescence excitation (PLE) bands at higher energy in Fig. 7 have a very good correspondence with the absorption bands of synthetic spessartine $[Mn_3Al_2(SiO_4)_3]$(Smith and Langer, 1983), with a difference of the peak maxima of −0.2 nm, −2.1 nm and 2.0 nm for the three bands (from lowest to highest), respectively. The same small differences have been observed also comparing with natural spessartine [21]. Concerning the two PLE bands at lower energy in Fig. 7, the difference with respect to the synthetic spessartine, −12 nm and −6.8 nm for the 451 nm and 474 nm bands, could be related to the difference of the crystal field, and thus of the transition energies, in

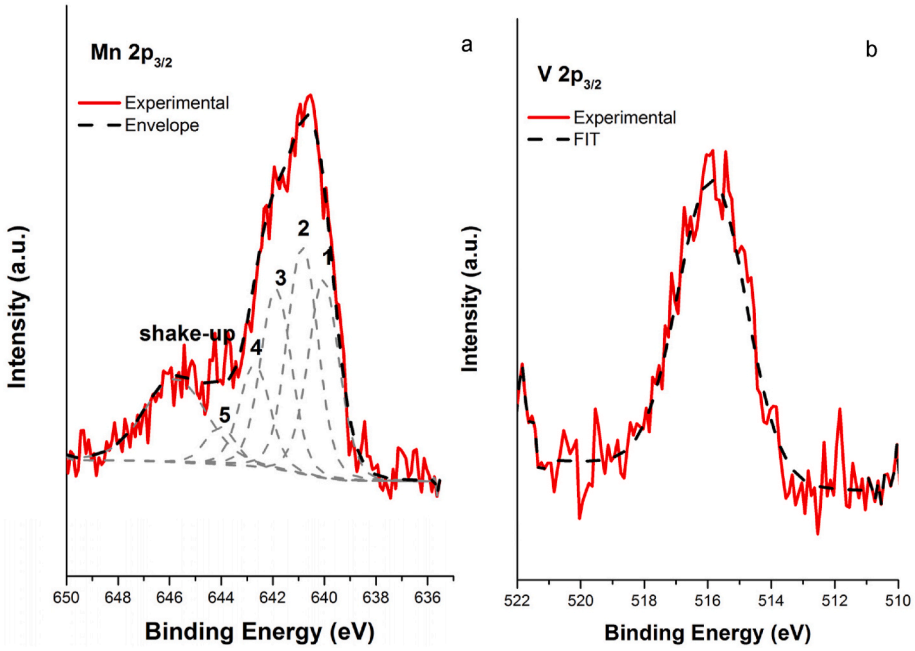

Fig. 5. a) Mn^{2+} $2p_{3/2}$ peak. Curve fitting according to Biesinger et al. (2011) and Grosvenor et al. (2016); b) V $2p_{3/2}$ peak recorded on the tsavorite sample.

Table 5
Recast of the garnet end-member molar composition of tsavorite.

End-member	$\{X\}_{dod.}[Y]_{oct.}(Z)_{tetr.}O_{12}$	Ts A1	Ts B1	Ts C6	Ts C1	Ts C2
Grossular	$\{Ca_3\}[Al_2](Si_3)O_{12}$	84.46 %	85.97 %	85.34 %	85.98 %	86.91 %
Goldmanite	$\{Ca_3\}[V_2](Si_3)O_{12}$	7.25 %	5.91 %	5.88 %	4.86 %	5.50 %
Spessartine	$\{Mn_3\}[Al_2](Si_3)O_{12}$	1.50 %	1.10 %	1.23 %	1.25 %	1.12 %
Morimotoite-Mg	$\{Ca_3\}[TiMg](Si_3)O_{12}$	/	1.45 %	1.24 %	1.46 %	1.59 %
Uvarovite	$\{Ca_3\}[Cr_2](Si_3)O_{12}$	1.19 %	1.55 %	0.95 %	1.36 %	1.24 %
Pyrope	$\{Mg_3\}[Al_2](Si_3)O_{12}$	1.30 %	0.71 %	0.10 %	0.23 %	0.63 %

Table 6
Crystallographic site occupancy of tsavorite.

Sample	Site	Si	OH	Ti	Al	Cr	V^{3+}	Mn^{2+}	Mg	Ca
TsA1	dodecahedral (X)							0.03	0.02	2.95
	octahedral (Y)			0.02	1.82	0.03	0.12			
	tetrahedral (Z)	2.90	0.10							
TsB1	dodecahedral (X)							0.04	0.02	2.87
	octahedral (Y)			0.02	1.82	0.02	0.14		0.02	
	tetrahedral (Z)	2.95	0.05							
TsC6	dodecahedral (X)							0.03	0.03	2.96
	octahedral (Y)	0.00		0.01	1.80	0.02	0.12		0.01	
	tetrahedral (Z)	2.93	0.70							
TsC1	dodecahedral (X)							0.04	0.01	2.96
	octahedral (Y)			0.01	1.82	0.03	0.10		0.03	
	tetrahedral (Z)	2.90	0.10							
TsC2	dodecahedral (X)							0.04	0.02	2.97
	octahedral (Y)			0.02	1.84	0.03	0.11		0.01	
	tetrahedral (Z)	2.94	0.10							

grossular and spessartine. The emission band at 591 nm could be generated by the $^4T_1$ (^4G) $\rightarrow$ $^6A_1$ (^6S) transition, that strongly depends on the strength of the crystal field (see the Tanabe-Sugano diagram reported in Fig. 8). This emission is detected at ~2.2 eV in synthetic garnets [23], close to the value here observed and reported in Table 7 (2.10 eV). However, as a consequence of the splitting of the degenerate excited states due to the lowering of symmetry with respect to the exact dodecahedral coordination (O_h symmetry point group), more absorption (or PLE) bands could be expected. In fact, the comparison between the observed and calculated emissions from the Tanabe-Sugano 3 d^5 ion indicates significant differences (Table 7)

The data reported in Table 7 are calculated considering the following values:

$\nu_1 = {}^6A_1 \rightarrow {}^4T_1({}^4G)$; 474 nm; 21097 cm^{-1}

$\nu\ 2 = {}^6A_1 \rightarrow {}^4T_2({}^4G)$; 451 nm; 22173 cm^{-1}

$\nu\ 2/\ \nu\ 1 = 1.05$;

Sliding into the 3 d^5 diagram (Fig. 8, we obtain: Dq/B = 4.19; E [$^4T_1$(^4G)]/B = 30.46; B = 693 cm^{-1} and Dq = 2904 cm^{-1} (Fig. 8).

From Table 7 it is evident that the observed transitions are not found in the expected E/B values of the Tanabe-Sugano diagram. Also, the stokes-shift between the $^4T_1$(^4G)$\rightarrow$$^6A_1$ emission and the $^6A_1$ $\rightarrow$$^4T_1$($^4G$) absorption is 4177 cm^{-1}, definitely too large a value. We agree with

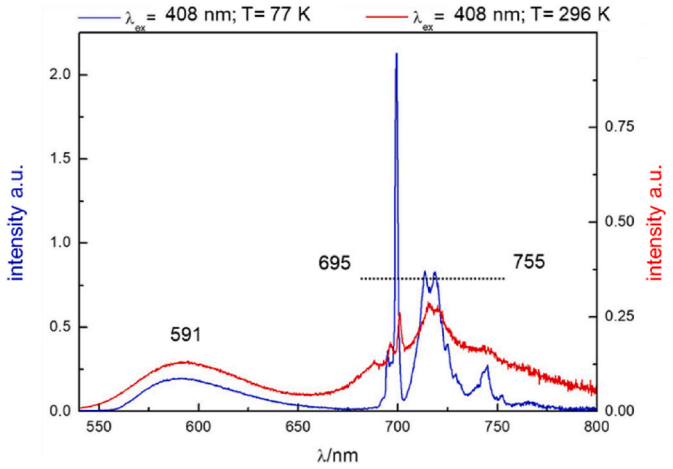

Fig. 6. Luminescence spectra of tsavorite under excitation light at 408 nm. The blue line is the observation at 77 K and the red line at a room temperature of 296 K.

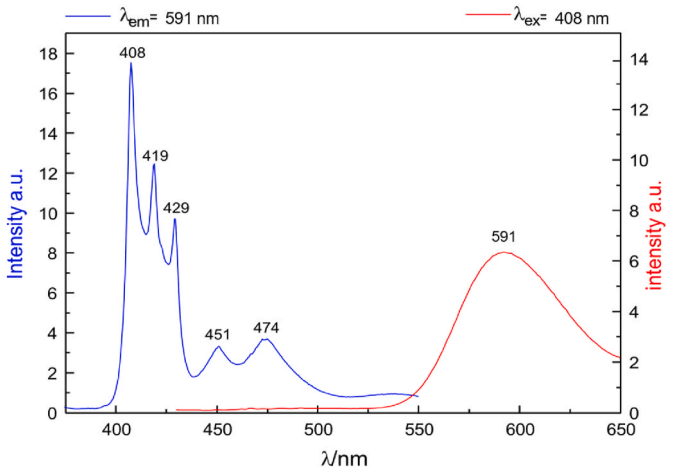

Fig. 7. Tsavorite garnet: excitation spectrum (blue line, λ_{em} = 591 nm) and emission spectrum (red line, λ_{ex} = 408 nm) in the 375–650 nm region at a room temperature of 296 K.

Smith & Langer (1983), Taran et al. [21] and Zhu et al. [24]: a more advanced model is necessary to achieve a full understanding of the possible energy transitions of a 3 d^5 metal ion in a distorted dodecahedral coordination, such as Mn^{2+} in tsavoriteMoreover, considering the possible optically active ions present in trace amounts in tsavorite [17,25], other emission centres could be overlapped by the emission of Mn^{2+} in the 591 nm broad band. To confirm or exclude any possible correlation with other elements (e.g. Fe, Fe-Ti, lanthanides, etc.), further observations based on synthetic grossular doped with Mn^{2+} and concerning the nature of the emission and excitation bands in the yellow region could be resolutive.

4.2. Far red region

The second region of emissions (695–755 nm) is composed of several convoluted bands at 296 K that become better resolved at 77 K (Fig. 9; Table 8).

The spectrum at 296 K is dominated by the asymmetric 716 nm and narrow 701 nm bands, with the first band more intense than the second one. At 77 K the relative intensities are opposite: moving from 296 K to 77 K the 701 nm maximum shifts to 699.2 nm (indicated with 2 in Fig. 9 and Table 8) and becomes the more intense emission, while the 716 nm

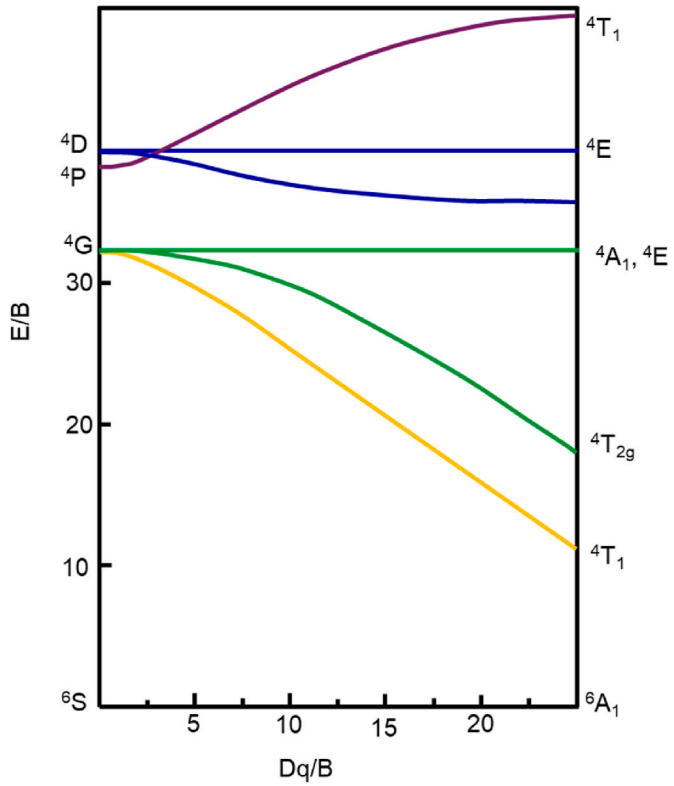

Fig. 8. Plot of the Tanabe-Sugano diagram for a 3 d^5 ion (Mn^{2+}). The vertical dashed line indicates the value of Dq/B for which the transition energies are those found in the present study (B = 693 cm^{-1}; Dq/B = 4.19).

band is resolved into two peaks at 713.6 nm (3) and 718.6 nm (4) and it becomes less strong compared to the band at 699.2 nm (2) (Fig. 9). Focusing on the spectrum at 77 K, the structure of these bands allows us to assign the 694.8 nm (1) and 699.2 nm (2) bands to the R-lines of Cr^{3+}, originated by the spin-orbit split $^2E(^2G) \rightarrow {}^4A_2\,(^4F)$ transition, that is one of the most studied emissions in inorganic spectroscopy (Henderson & Imbush, 1989). These emission bands, numbered from (3) to (8) at 77 K, have been observed in many research studies and have been the subject of different assignments, such as sidebands of the Cr^{3+} R-lines [9,26], or caused by the V^{2+} ion [11]. The presence of V^{2+} in tsavorite has been excluded by XPS (present work), EPR [8] and by K-edge XAS analyses [12]. In order to understand if these emissions are generated, or not, by the same emission centre responsible for the R-lines (Cr^{3+}), the excitation spectra with λ_{em} equal to 688 nm, 697 nm, 701 nm, 716 nm, and 741 nm were acquired (Fig. 10).

The results indicate that all the emission bands (1)–(8) in the far red region are pumped by the same excitation wavelengths at 442 nm (22624 cm^{-1}) and 603 nm (16584 cm^{-1}) corresponding to the $^4A_2(^4F) \rightarrow {}^4T_1(^4F)$, $^4A_2(^4F) \rightarrow {}^4T_2(^4F)$ transitions of Cr^{3+}, see Fig. 10 [27]. Noticeably, in the excitation spectrum of the 741 nm emission, it is possible to recognize a couple of weak and narrow absorption bands pairing the R1 and R2 lines observed at 77 K and due to the spin-forbidden absorption transitions to the split $^2E(^2G)$ states [28,29]. Using three transitions it is possible to calculate the B and C Racah parameters and the crystal-field splitting parameter Dq for 3 d^3 metal ions (Henderson & Imbush, 1989) from the equations [29,30],:

$$10Dq = E[^4A_2(^4F) \rightarrow {}^4T_2(^4F)] \quad (1)$$

$$\Delta E = E[^4T_1(^4F)]\text{-}E[^4T_2(^4F)] \quad (2)$$

$$Dq/B = 15[(\Delta E/Dq)\text{-}8]/\,[(\Delta E/Dq)^2 \text{-}10(\Delta E/Dq)] \quad (3)$$

$$^2E(^2G) = 3.05C + 7.90B\ 1.80B^2/Dq \quad (4)$$

Table 7
Observed energy transition of Mn^{2+} in tsavorite and calculated transition of a 3 d^5 ion in O_h point symmetry.

observed transitions				calculated transitions			
λ(nm)	ν (cm^{-1})	eV		λ(nm)	ν (cm^{-1})	eV	
591em	16920	2.1	$^4T_1(^4G)\rightarrow{}^6A_1$				
474ex	21097	2.61	$^6A_1\rightarrow{}^4T_1(^4G)$	474	21097	2.62	$^6A_1\rightarrow{}^4T_1(^4G)$
451ex	22173	2.75	$^6A_1\rightarrow{}^4T_2(^4G)$	451	22173	2.75	$^6A_1\rightarrow{}^4T_2(^4G)$
429ex	23310	2.89	?	445	22472	2.79	$^6A_1\rightarrow{}^4A_1(^4G)/^4E(^4G)$
419ex	23866	2.96	?	360	27778	3.44	$^6A_1\rightarrow{}^4T_1(^4P)$
408ex	24630	3.05	?	372	26882	3.33	$^6A_1\rightarrow{}^4T_2(^4D)$
				366	27322	3.39	$^6A_1\rightarrow{}^4E(^4D)$

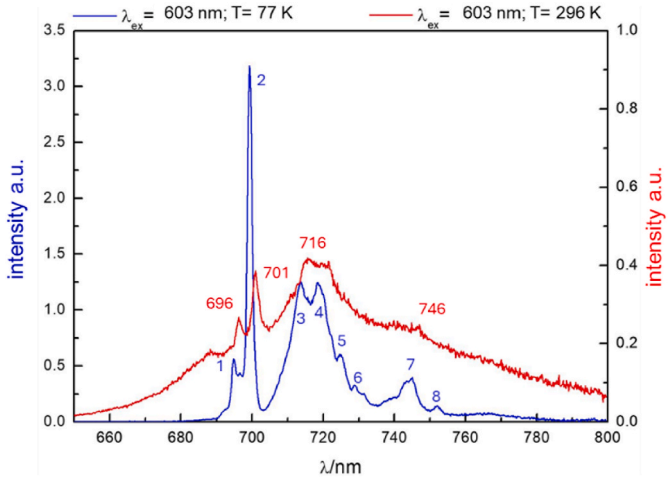

Fig. 9. Emission spectrum of tsavorite (λ_{ex} = 603 nm) at 77 K (blue line) and 296 K (red line).

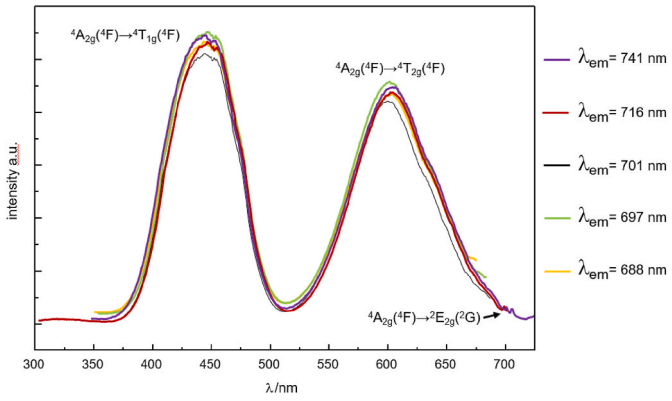

Fig. 10. Excitation bands of the Cr^{3+} emissions.

Table 8
Tsavorite emissions in the far-red region.

	λ_{ex} = 603 nm (77 K)			λ_{ex} = 603 nm (296 K)		
	λ_{em} (nm)	cm^{-1}	eV	λ_{em} (nm)	cm^{-1}	eV
1	694.8	14393	1.784	696	14368	1.781
2	699.2	14302	1.773	701	14265	1.769
3	713.6	14013	1.737	716	13966	1.732
4	718.6	13916	1.725			
5	724.6	13801	1.711	/	/	/
6	728.8	13721	1.701	/	/	/
7	745.0	13423	1.664	746	13405	1.662
8	752.0	13298	1.649	/	/	/

resulting in Dq = 1658.4 cm^{-1}; Dq/B = 2.83; B = 587 cm^{-1}; C = 3291 cm^{-1}, computed from the values 14302 cm^{-1}, 16584 cm^{-1}, and 22624 cm^{-1} for the $^4A_2(^4F)\rightarrow{}^2E(^2G)$, $^4A_2(^4F)\rightarrow{}^4T_2(^4F)$, and $^4A_2(^4F)\rightarrow{}^4T_1(^4F)$ transitions, respectively. This method [30] calculates directly the Racah parameter C, hence avoiding the use of a fixed C/B ratio, as usually done. The 3 d^3 Tanabe-Sugano diagram for the Dq and B values is reported in Fig. 11. One promptly notes that the crystal field in tsavorite is strong (Dq/B = 2.83) and slightly larger than the value at which the $^2E(^2G)$ and $^4T_2(^4F)$ energies cross (Dq/B = 2.42). This result indicates that the emissions observed at 77 K (1)(2) (Fig. 9 and Table 8) are due to the $^2E(^1G)\rightarrow{}^4A_2(^4F)$ transition (two lines are observed as a consequence of the spin-orbit splitting of the $^2E(^2G)$ level) and also suggests that the emissions from (3) to (8) are its sideband.

However, by increasing the temperature from 77 K to 296 K the emissions (3) and (4) become broader, peaking at 716 nm: this could be due in part to the overlap of the bands observed at 77 K with the $^4T_2(^4F)\rightarrow{}^4A_2(^4F)$ emission, as explained by Struve & Hubner [31], where it is shown that in synthetic garnet YGG:Cr^{3+} the $^4T_2(^4F)$ state can be close in energy to the $^2E(^2G)$ state, or even slightly lower, in case of large

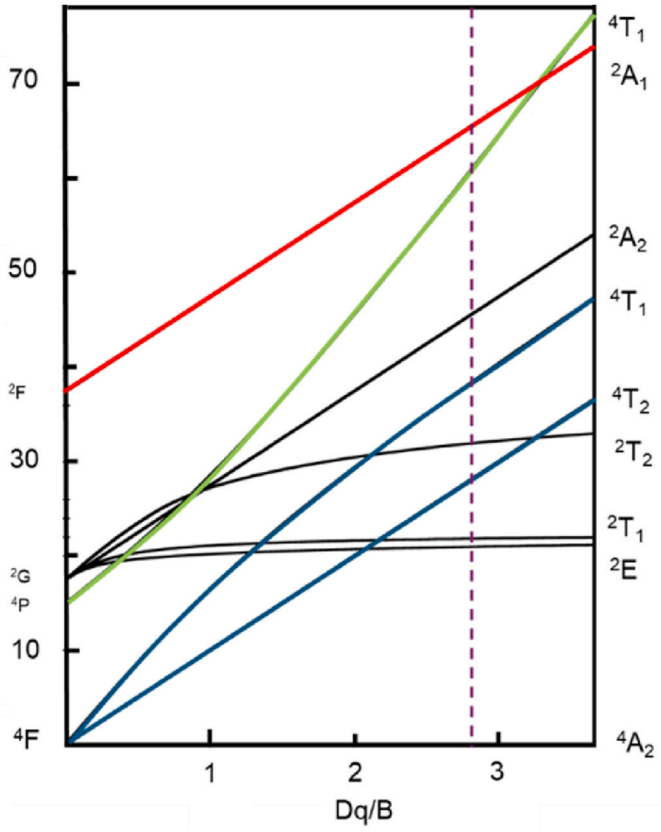

Fig. 11. Portion of the 3 d^3 Tanabe Sugano diagram in O_h octahedral symmetry calculated for Cr^{3+} in Tsavorite according to the method of Song et al [30]. Only the states relevant to the discussion are labelled.

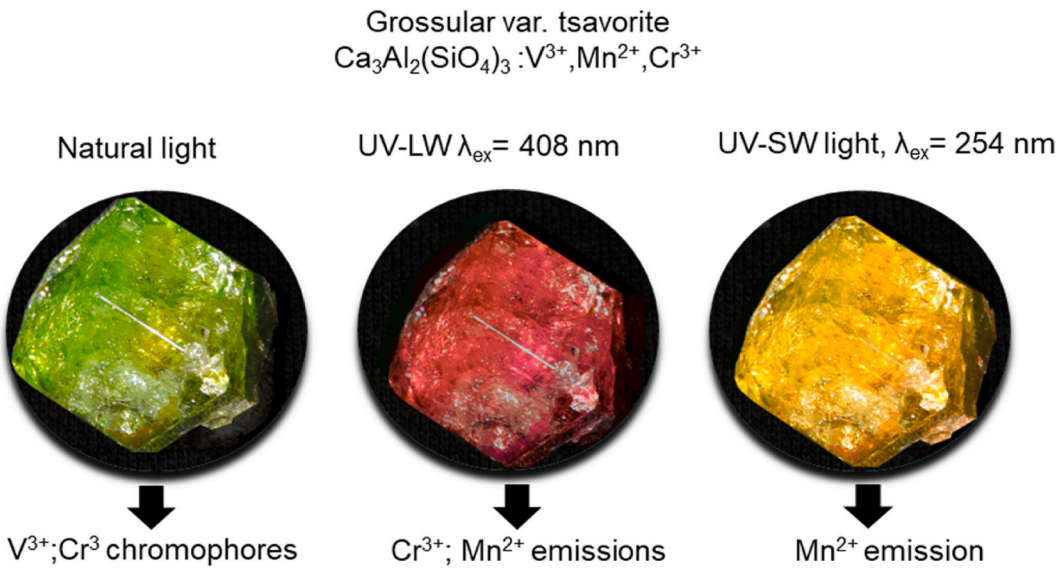

Fig. 12. Colour and fluorescence colors of tsavorite from Merelani Hills, Tanzania. On the left under natural light, in the center under UV-longwave light (λ_{ex} = 408 nm) and on the right under shortwave light (λ_{ex} = 254 nm).

stokeshift. At room temperature, the intersystem crossing $^4T_2(^4F) \rightarrow ^2E(^2G)$ could not have unit efficiency leaving a residual spin allowed radiative transition $^4T_2(^4F) \rightarrow {}^4A_2(^4F)$ at higher energy with respect to the doublet emission [28]. It should be noted that in the synthetic garnet the Cr $^{3+}$ emissions are tunable varying the temperature, and this phenomenon is related to the thermal population of the ^2E and $^4T_2$ [32] in analogy with what we observe in tsavorite. Co-existence of both emissions has been described also by Dereń et al. [33] in synthetic garnet (YGG:Cr^{3+}) and by Cao et al. [34] in synthetic perovskite (Ca_2AlNbO_6:Cr^{3+}). This "intermediate" behavior has been observed in other minerals such as alexandrite and emerald [28] in spite of the fact that in both minerals the chromophore is in a strong crystal field. In the extensive research of Adachi [27,35–38] the determination of the Racah parameters is performed by finding the zero-phonon line energy of each transition, rather than taking the maximum of the peaks in the absorption/excitation spectrum. Such a procedure is slightly more involved, requiring for each transition the presence and the clear identification of the vibronic (phononic) bands in both the excitation and emission spectra and a multiparameter fitting procedure of these bands. We plan to perform such a study in a future work also including synthetic garnet, moreover enhancing and deepening the analysis of the luminescence nature of tsavorite with the determination of the life times of the emissions.

5. Concluding remarks

Grossular garnet var. tsavorite from Merelani Hills, Tanzania, is a fluorescent mineral. The characteristic green color under natural light is caused by the V^{3+} and Cr^{3+} chromophores. When illuminated with shortwave and longwave UV light, the crystals exhibit yellow and red colors (Fig. 12).

The chemical composition of the gem quality crystals indicates that this variety of garnet is composed by O > Ca > Si > Al as major elements and V > Mn > Cr ~ Mg ~ Ti as minor elements. The oxidation state of Mn is +2, the oxidation state of V is +3. Hence, the garnet end-member composition of tsavorite is grossular (~85 mol%), goldmanite (~6 mol %), spessartine (~1 mol%) and minor amounts of uvarovite, pyrope and morimotoite. The emission in the yellow region (591 nm) is caused by Mn^{2+} at both 296 K and 77 K, with the excitation spectrum of the 591 nm emission composed by five bands (474, 451, 429, 419 and 408 nm), in analogy to those of synthetic spessartine. Manganese in tsavorite occupies a dodecahedral distorted site (D_2 point symmetry), and its transitions are not simply interpretable using the Tanabe-Sugano diagram based on the O_h point symmetry. The emission in the red region at room temperature is composed by four bands peaking at 746, 716 701 and 696 nm, while at 77 K the bands become more resolved. The excitation spectra clearly point out to a single origin of all emissions in the red region. Comparing the experimental data with the literature, it can be said that the red emission is caused by the $^2E(^2G) \rightarrow {}^4A_2(^4F)$ transitions of Cr^{3+} in a strong crystal field at 77 K, while at 296 K the contribution of $^4T_2(^4F) \rightarrow {}^4A_2(^4F)$ emission is probably also observed. Finally, one can state that the presence of V^{2+}, and its role as emission center in tsavorite, must be discarded. Subsequently, the bibliographic attribution to V^{2+} of the red emissions in other natural silicate must be proved using other analytical techniques.

Taking into account the elemental complexity of natural samples in terms of minor and trace elements, further studies based on synthetic analogue of tsavorite could be very useful to continue the investigations of garnet luminescence property.

CRediT authorship contribution statement

A. Idini: Writing – review & editing, Writing – original draft, Methodology, Investigation, Formal analysis, Data curation, Conceptualization. **R. Argazzi:** Writing – review & editing, Methodology, Investigation, Formal analysis. **F. Frau:** Writing – review & editing, Validation, Supervision, Conceptualization. **M. Fantauzzi:** Writing – review & editing, Methodology, Formal analysis, Data curation. **C. Angeli:** Writing – review & editing, Supervision, Methodology, Investigation, Conceptualization.

Declaration of competing interest

The authors declare that they have no known competing financial interests or personal relationships that could have appeared to influence the work reported in this paper.

Acknowledgements and fundings

This work has been developed within the framework of the project e. INS- Ecosystem of Innovation for Next Generation Sardinia (cod. ECS 00000038) funded by the Italian Ministry for Research and Education (MUR) under the National Recovery and Resilience Plan (NRRP) - MISSION 4 COMPONENT 2, "From research to business" INVESTMENT

1.5, "Creation and strengthening of Ecosystems of innovation" and construction of "Territorial R&D Leaders". Funding from the projects - “Poseidonia2022”- Autorità portuale Mare di Sardegna- Prof. Pascucci J13C23000380005.- “Amp2023pascucci” -Area marina protetta Capo Caccia e Isola Piana- Prof. Pascucci B21G11000040001. - “FDS2017OGGIANO” -Fondazione di Sardegna- Prof. Oggiano, Prof. Mameli J85F21000970005.

Appendix A. Supplementary data

Supplementary data to this article can be found online at https://doi.org/10.1016/j.jlumin.2024.120936.

Data availability

Data will be made available on request.

References

[1] I. Adamo, V. Diella, F. Pezzotta, Tsavorite and other grossulars from itrafo, Madagascar, Gems Gemol. 48 (3) (2012) 178–187, https://doi.org/10.5741/GEMS.48.3.178.

[2] A. Idini, C. Angeli, F. Frau, G. Ennas, S. Naitza, G.B. De Giudici, R. Argazzi, Mineralogical characterization of fluorescent grossular garnet var. tsavorite from Merelani Hills, Tanzania, Phys. Chem. Miner. 50 (1) (2023), https://doi.org/10.1007/s00269-023-01233-w.

[3] B. Cairncross, Connoisseur’s choice: tsavorite, the green gem variety of grossular, Merelani Hills, manyara district, Tanzania, Rocks Miner. 95 (3) (2020) 252–259, https://doi.org/10.1080/00357529.2020.1716171.

[4] Y. Ma, Y. Guo, Variation in gemological characteristics in tsavorites with different tones from east africa, Crystals 12 (11) (2022), https://doi.org/10.3390/cryst12111677.

[5] K. Suwa, K. Suzuki, T. Agata, Vanadium grossular from the Mozambique metamorphic rocks, south Kenya, J. Southeast Asian Earth Sci. 14 (3–4) (1996) 299–308, https://doi.org/10.1016/S0743-9547(96)00066-9.

[6] Julien Feneyrol, D. Ohnenstetter, G. Giuliani, A.E. Fallick, C. Rollion-Bard, J. L. Robert, E.P. Malisa, Evidence of evaporites in the genesis of the vanadian grossular “tsavorite” deposit in Namalulu, Tanzania, Can. Mineral. 50 (3) (2012) 745–769, https://doi.org/10.3749/canmin.50.3.745.

[7] B.C. Hoare, S.E. Arden, G.J. O’Sullivan, U–Pb dating of gem-quality vanadium-bearing grossular garnet (var. tsavorite) from north-eastern Tanzania, Miner. Deposita 59 (2) (2024) 419–431, https://doi.org/10.1007/s00126-023-01206-7.

[8] Q. Zhang, Y. Shi, T. Shao, X. Li, F. Xu, A.H. Shen, Luminescence characteristics of green grossular garnets, Minerals 13 (5) (2023), https://doi.org/10.3390/min13050639.

[9] Z. Mazurak, M. Czaja, Optical properties of tsavorite $Ca_3Al_2(SiO_4)_3$:Cr^{3+},V^{3+} from Kenya, J. Lumin. 65 (6) (1995) 335–340, https://doi.org/10.1016/0022-2313(95)00086-0.

[10] M. Czaja, Z. Mazurak, Crystal-field analysis of Cr^{3+} in grossular $Ca_3Al_2(SiO_4)_3$, Opt. Mater. 3 (2) (1994) 95–98, https://doi.org/10.1016/0925-3467(94)90012-4.

[11] M. Gaft, H. Yeates, L. Nagli, G. Panczer, Laser-induced time resolved luminescence of natural grossular $Ca_3Al_2(SiO_4)_3$, J. Lumin. 137 (2013) 43–53, https://doi.org/10.1016/j.jlumin.2012.11.015.

[12] A. Bordage, C. Brouder, E. Balan, D. Cabaret, A. Juhin, M.A. Arrio, P. Sainctavit, G. Calas, P. Glatzel, Electronic structure and local environment of substitutional V^{3+} in grossular garnet Ca3Al2(SiO4)3: K-edge X-ray absorption spectroscopy and first-principles modeling, Am. Mineral. 95 (8–9) (2010) 1161–1171, https://doi.org/10.2138/am.2010.3432.

[13] M. Gaft, W. Strek, L. Nagli, G. Panczer, G.R. Rossman, L. Marciniak, Laser-induced time-resolved luminescence of natural sillimanite Al_2SiO_5 and synthetic Al_2SiO_5 activated by chromium, J. Lumin. 132 (11) (2012) 2855–2862, https://doi.org/10.1016/j.jlumin.2012.04.045.

[14] K. Schmetzer, Absorptions- und Emissionsspektrum von V^{2+}/V^{3+} in Beryllen, 1974, pp. 3–5. Smith. (n.d.).

[15] N. Ollier, Y. Fuchs, O. Cavani, A.H. Horn, S. Rossano, Influence of impurities on Cr^{3+} luminescence properties in Brazilian emerald and alexandrite, Eur. J. Mineral 27 (6) (2015) 783–792, https://doi.org/10.1127/ejm/2015/0027-2484.

[16] J. Feneyrol, G. Giuliani, D. Ohnenstetter, A.E. Fallick, J.E. Martelat, P. Monié, J. Dubessy, C. Rollion-Bard, E. Le Goff, E. Malisa, A.F.M. Rakotondrazafy, V. Pardieu, T. Kahn, D. Ichang’i, E. Venance, N.R. Voarintsoa, M.M. Ranatsenho, C. Simonet, E. Omito, M. Saul, New aspects and perspectives on tsavorite deposits, Ore Geol. Rev. 53 (November 2012) (2013) 1–25, https://doi.org/10.1016/j.oregeorev.2013.01.016.

[17] Julien Feneyrol, G. Giuliani, D. Ohnenstetter, B. Rondeau, E. Fritsch, A.E. Fallick, D. Ichang’i, E. Omito, M. Rakotondrazafy, M. Ranatsenho, F. Lallier, New typology and origin of tsavorite based on trace-element chemistry, Eur. J. Mineral 26 (2) (2014) 293–308, https://doi.org/10.1127/0935-1221/2014/0026-2367.

[18] E.S. Grew, A.J. Locock, S.J. Mills, I.O. Galuskina, E.V. Galuskin, U. Hålenius, IMA report: nomenclature of the garnet supergroup, Am. Mineral. 98 (4) (2013) 785–810, https://doi.org/10.2138/am.2013.4201.

[19] A.J. Locock, An Excel spreadsheet to recast analyses of garnet into end-member components, and a synopsis of the crystal chemistry of natural silicate garnets, Comput. Geosci. 34 (12) (2008) 1769–1780, https://doi.org/10.1016/j.cageo.2007.12.013.

[20] L. Dong, L. Zhang, Y. Jia, B. Shao, W. Lü, S. Zhao, H. You, Site occupation and luminescence of novel orange-red $Ca_3M_2Ge_3O_{12}$:Mn^{2+},Mn^{4+} (M = Al, Ga) phosphors, ACS Sustain. Chem. Eng. 8 (8) (2020) 3357–3366, https://doi.org/10.1021/acssuschemeng.9b07281.

[21] M.N. Taran, C.A. Geiger, O.A. Vyshnevskyi, G.R. Rossman, Single-crystal UV/Vis optical absorption spectra of almandine-bearing and spessartine garnet: Part II. An analysis of the spin-forbidden bands of Fe^{2+}, Mn^{2+}, and Fe^{3+}, Am. Mineral. 108 (6) (2023) 1161–1170, https://doi.org/10.2138/am-2022-8500.

[22] R.G. Burns, Outline of crystal field theory, in: Mineralogical Applications of Crystal Field Theory, 2009, https://doi.org/10.1017/cbo9780511524899.004.

[23] Q. Chen, M. Liu, L. Shang, C.K. Duan, Elucidating the multisite and multivalence nature of Mn ions in solids and predicting their optical transition properties: a case study on a series of garnet hosts, Inorg. Chem. 61 (46) (2022) 18690–18700, https://doi.org/10.1021/acs.inorgchem.2c03175.

[24] X. Zhu, S. Zhang, S. Ye, Does Mn^{2+}-Mn^{2+} spin-exchange interaction involve Mn2+ luminescence of Mn2+-doped/concentrated materials? J. Phys. Chem. Lett. 15 (10) (2024) 2804–2814, https://doi.org/10.1021/acs.jpclett.3c03581.

[25] H. Chen, R.W. Stimets, Fluorescence of trivalent neodymium in various materials excited by a 785 nm laser, Am. Mineral. 99 (2–3) (2014) 332–342, https://doi.org/10.2138/am.2014.4311.

[26] B. Struve, G. Huber, The effect of the crystal field strength on the optical spectra of Cr^{3+} in gallium garnet laser crystals, Appl. Phys. B 36 (4) (1985) 195–201, https://doi.org/10.1007/BF00704574.

[27] S. Adachi, Review—photoluminescence properties of C $^{3+}$ -activated oxide phosphors, ECS Journal of Solid State Science and Technology 10 (2) (2021) 026001, https://doi.org/10.1149/2162-8777/abdc01.

[28] J.G. Solé, L.E. Bausá, D. Jaque, Applications: rare earth and transition metal ions, and color centers, in: An Introduction to the Optical Spectroscopy of Inorganic Solids, vol. 6, 2005, https://doi.org/10.1002/0470016043.ch6.

[29] M.G. Brik, A.M. Srivastava, Critical review—a review of the electronic structure and optical properties of ions with d 3 electron configuration (V^{2+} , Cr^{3+} , Mn^{4+} , Fe^{5+}) and main related misconceptions, ECS Journal of Solid State Science and Technology 7 (1) (2018) R3079–R3085, https://doi.org/10.1149/2.0041801jss.

[30] Z. Song, P.A. Tanner, Q. Liu, Host dependency of boundary between strong and weak crystal field strength of Cr^{3+} luminescence, J. Phys. Chem. Lett. 15 (2024) 2319–2324, https://doi.org/10.1021/acs.jpclett.4c00008.

[31] B. Struve, G. Huber, V.V. Laptev, I.A. Shcherbakov, E.V. Zharikov, Tunable room-temperature cw laser action in Cr^{3+}: GdScGa-Garnet, Appl. Phys. B 30 (3) (1983) 117–120, https://doi.org/10.1007/BF00695465.

[32] J. Zhou, T. Ye, Q. Zhu, J. Huo, Q. Zhang, Achieving ultrahigh thermal stability in Cr^{3+}-activated garnet phosphors through electron migration between thermally coupled levels, Inorg. Chem. 63 (31) (2024) 14665–14672, https://doi.org/10.1021/acs.inorgchem.4c02239.

[33] P.J. Dereń, A. Watras, A. Gągor, R. Pązik, Weak crystal field in yttrium gallium garnet (YGG) submicrocrystals doped with Cr^{3+}, Cryst. Growth Des. 12 (10) (2012) 4752–4757, https://doi.org/10.1021/cg300435t.

[34] R. Cao, J. Tang, J. Nie, C. Liao, Y. Cao, L. Li, R. Liu, J. Wang, Synthesis and luminescent performances of Ca_2AlNbO_6:Cr^{3+} perovskite phosphor, J. Mol. Struct. 1318 (P2) (2024) 139351, https://doi.org/10.1016/j.molstruc.2024.139351.

[35] S. Adachi, Photoluminescence spectroscopy and crystal-field parameters of Cr^{3+} ion in red and deep red-emitting phosphors, ECS Journal of Solid State Science and Technology 8 (12) (2019) R164–R168, https://doi.org/10.1149/2.0061912jss.

[36] S. Adachi, Luminescence spectroscopy of Cr^{3+} in an oxide: a strong or weak crystal-field phosphor? J. Lumin. 234 (January) (2021) 117965 https://doi.org/10.1016/j.jlumin.2021.117965.

[37] S. Adachi, Spectroscopy of Cr^{3+} activator: Tanabe−Sugano diagram and Racah parameter analysis, J. Lumin. 232 (December 2020) (2021) 117844, https://doi.org/10.1016/j.jlumin.2020.117844.

[38] S. Adachi, Luminescence spectroscopy of $3d^3$ (Mn^{4+} , Cr^{3+}) ions in multiple octahedral-site phosphors, ECS Journal of Solid State Science and Technology 11 (4) (2022) 046002, https://doi.org/10.1149/2162-8777/ac63e4.